Geophysical Journal International

Geophys. J. Int. (2025) **240,** 317–328
Advance Access publication 2024 October 26
GJI Seismology
https://doi.org/10.1093/gji/ggae380

Temporal variation of *S*-wave attenuation during the 2009 L'Aquila, Central Italy, seismic sequence

Raúl R. Castro [1], Leonardo Colavitti [2,3] Francesca Pacor [2] Giovanni Lanzano [2] Sara Sgobba [2] and Daniele Spallarossa [3]

[1] *Departamento de Sismología, División Ciencias de la Tierra, Centro de Investigación Científica y de Educación Superior de Ensenada (CICESE), Ensenada, Baja CA 22860, México. E-mail: raul@cicese.mx*
[2] *Departamenti Terremoti, Istituto Nazionale di Geofisica e Vulcanologia, Sezione di Milano, 20133 Milan, Italy. E-mail: leonardo.colavitti@edu.unige.it*
[3] *Department of Earth, Environment and Life Sciences – DISTAV, University of Genoa, 16132 Genoa, Italy*

Accepted 2024 October 15. Received 2024 September 14; in original form 2023 December 19

SUMMARY

We investigate temporal and spatial variations of the spectral decay parameter kappa (κ) before and after the 6 April 2009, L'Aquila earthquake (M_w 6.1), in Central Italy. We analysed foreshocks 10 days before and aftershocks occurring 10 days and 6 months after this main event. We select earthquakes with magnitudes $M_w \geq 3.2$ registered by the seismic network of Central Italy within a radius of 20 km from the epicentre of the L'Aquila main shock and having hypocentre distances of less than 170 km. We separate near-source, along-path and near-site contributions of κ for each group of events and we detected temporal variations of this *S*-wave attenuation parameter. We find that 10 days before the main shock κ along the path has the lowest values, probably due to high tectonic stress accumulated, in agreement with previous investigations performed with other techniques, then κ increases during the main event and remains constant during the first 10 days of aftershocks. The aftershocks that occurred 6 months after show an increase in the regional attenuation probably due to the tectonic stress released during the main shock and the earlier aftershocks. From the spatial point of view, 10 days before the principal event the foreshocks located to the south show an increase in the near-source attenuation towards the northeast, in the direction of the main shock. These spatial variations of κ may be related to the presence of crustal fluids near the rupture area, as evidenced by other previous studies. The first 10 days of aftershocks that concentrate around the main earthquake have high near-source κ, and those located north of the main rupture have lower values. These observations are consistent with previous investigations that show variations of elastic and anisotropic crustal properties during the L'Aquila earthquake sequence due to dilatancy and fluid diffusion processes within the nucleation zone. We conclude that temporal variations of the spectral decay parameter κ provide important clues for the earthquake cycle in Central Italy.

Key words: Body waves; Earthquake source observations; Seismic attenuation.

INTRODUCTION

On 6 April 2009, an earthquake magnitude M_w 6.1 (INGV-CNT Seismic Bulletin and Herrmann *et al.* 2011) occurred near the city of L'Aquila, Central Italy, destroying and damaging thousands of buildings, causing 300 deaths and about 1000 injuries (Walters *et al.* 2009; Calderoni *et al.* 2015). Geological and geophysical investigations (Falcucci *et al.* 2009; Chioccarelli & Iervolino 2010; Chiaraluce *et al.* 2011; Tinti *et al.* 2014) have found that the Paganica fault, a NW–SE-striking and SW-dipping Quaternary normal fault located east of L'Aquila, was the most likely structure responsible for the main event. The 20-km-long rupture (Chiarabba *et al.* 2009), propagated up dip, unilaterally along the strike of the Paga-nica fault, towards the southeast (Chioccarelli & Iervolino 2010; Ameri *et al.* 2012; Gallovič & Zahradník 2012; Tinti *et al.* 2014). Before the main shock of April 2009, Borghi *et al.* (2016) identified a slow-slip earthquake (M_w 5.9), that occurred on 12 February 2009, from a rigorous analysis of continuous GPS data. The slow-slip event lasted approximately 2 weeks and triggered a sequence of foreshocks generated by the faults of the region

(Lucente *et al.* 2010; Chiaraluce *et al.* 2011; Valoroso *et al.* 2013). More recently, Cabrera *et al.* (2022) analysed spatial-temporal patterns of foreshocks, based on physical parameters such as seismic moment release, stress drop and others and identified two foreshock sequences. They observed that the first one is characterized by weak earthquake interactions, low stress drops and aseismic processes. During the second part of the sequence, the foreshocks exhibit faster seismic expansion and a stress transfer process. Other studies indicate that this earthquake sequence was likely connected to overpressurized pore fluid around the fault before failure, leading various authors to infer a strong role of fluids in the earthquake nucleation (Di Luccio *et al.* 2010; Lucente *et al.* 2010; Terakawa *et al.* 2010). Moreover, in the following months the region was hit by many aftershocks (Chiarabba *et al.* 2009; Valoroso *et al.* 2013) that spread along a 40-km-long fault system (Malagnini *et al.* 2012). In a recent investigation based on a more complete catalogue of foreshocks and aftershocks Fonzetti *et al.* (2024) found significant temporal changes of V_p and V_p/V_s through a tomography technic. Their joint interpretation of the V_P and V_S tomography images may trace the presence of a fluid-saturated volume.

Several studies of focal mechanisms indicate normal faulting with ruptures along the strike in the NW–SE direction and dipping to the southwest (Scognamiglio *et al.* 2010; Herrmann *et al.* 2011; D'Amico *et al.* 2013). Calderoni *et al.* (2015) analysed rupture directivity of 70 earthquakes of the L'Aquila 2009 sequence and found a preferred rupture direction to the southeast on the L'Aquila fault. They suggest that possible mechanisms that could favour this rupture are related to the presence of fluids, persistent stress gradient and fault plane curvature. Chiarabba *et al.* (2022) observed changes of *P*-wave velocity (V_P) and the ratio V_P/V_S during the 2009 L'Aquila earthquake sequence that indicates a post-failure fluid migration. One of the main forces that prevent faults from slipping is due to the weight of the surrounding rocks which produce pressure and increases lateral stress on the fault, and the pore pressure of crustal fluids that reduce the necessary stress for rock failure and fault slipping (Savage 2010). Few studies have quantified the relation between fluid flow and earthquake sequences and the 2009 L'Aquila seismic sequence is an interesting testing ground that offers this opportunity.

Lucente *et al.* (2010) measured the ratio of *P*-to-*S* velocity and seismic anisotropy and showed that temporal variations of these parameters are caused by fluid flow within the foreshock region. Additional evidence was provided by Terakawa *et al.* (2010), who mapped fluid pressure inferred from focal mechanisms. Their maps show the presence of high overpressure fluids near the foreshock and the main shock regions, suggesting that high pore fluid pressures triggered the main shock. Fluid involvement in earthquake triggering is evidenced even by small changes in fluid pressure (Sibson 1992; Townend 2006). The coincidence between the areas of high fluid concentration found by Lucente *et al.* (2010) and the zones of high pore pressure determined by Tarakawa *et al.* (2010) reinforce the idea that circulation of fluids plays a crucial role in earthquake generation (Savage 2010).

Temporal changes of subsurface seismic velocities, related to earthquakes, have been reported by Poupinet, Ellsworth & Frednet (1984); Peng & Ben-Zion (2006); Niu *et al.* (2008); among others. These temporal variations of seismic velocities provide important information about possible pre, -co and post-earthquake effects as well as changes due to seasonal variations (Li & Ben-Zion 2023). Following the 2019 Mw 7.1 Ridgecrest, California earthquake, Lu & Ben-Zion (2022) analysed regional transient changes of seismic velocities that show regional coseismic velocity drops of about 2% in the first three km and about 8% near the Coso geothermal region. Time–space variations of seismic velocity using small earthquakes have also been reported. For instance, Bonilla & Ben-Zion (2021) detected apparent velocity changes at high frequencies (10–40 Hz) in the proximity of the San Jacinto fault, California. Most of these studies concluded that the observed changes are dominated by effects occurring in the very shallow crust.

Temporal changes in the attenuation of coda waves have been documented in California during earthquake sequences (Chouet 1979; Beroza *et al.* 1995) and in other parts of the world like Zagros mountains chain (Gholamzadeh *et al.* 2013) and Central Italy (Del Pezzo & Zollo 1984). For instance, Jin & Aki (1986) observed temporal changes in coda *Q* before the 1975 Haicheng and the 1976 Tangshan, China earthquakes. This variability of seismic velocity and attenuation during earthquake sequences have also been attributed to temporal changes of crustal rocks properties (Got *et al.* 1990).

Regarding the 2009 L'Aquila sequence, the velocity variation in the proximity to the fault zone was investigated by Soldati *et al.* (2015) using seismic noise and a cross-correlation technique. These authors observed a decrease of seismic velocity during the coseismic episode of the sequence that extended up to 40 km from the epicentre of the main shock. In a more recent study, Poli *et al.* (2020) also analysed velocity variations in the region surrounding L'Aquila using variable coda waves lapse time over a period of 17 yr. They observed velocity variations over multiple spatial and time scales, and their findings suggest the existence of fluid-filled cracks deep in the crust.

Moreover, several studies in Central Italy have been carried out analysing the temporal distribution of seismicity and attenuation from different earthquake sequences and the possible connection to deep fluid circulation (Castro *et al.* 2022b; Gabrielli *et al.* 2023) and to the triggering of multi-main shocks (Malagnini *et al.* 2022), particularly during the 2016–2017 Amatrice-Visso-Norcia sequence. These results agree with those of Picozzi *et al.* (2022a), who showed that the spatial and temporal distribution of the energy index (the deviation of the observed radiated energy with respect to theoretical values) of microearthquakes (M_w 1.8–3.5) of Central Italy region is a valuable indicator of crustal stress conditions. In another investigation, Picozzi *et al.* (2022b) highlighted that, starting from the months following the 2009 L'Aquila earthquake, a progressive northward diffusion of microseismicity was characterized by low energy index values.

Castro *et al.* (2022b) observed temporal variations of the spectral decay parameter kappa (κ) (Anderson & Hough 1984) during the Amatrice (M_w 6.0) of 24 August 2016, and the Norcia (M_w 6.5) of 30 October 2016, earthquake sequences in Central Italy and they suggested that spatial variability of tectonic stress and fluid flow could explain the observed temporal changes of high-frequency *S*-wave attenuation. However, because the Amatrice and the Norcia earthquakes are close to each other in both space and time, it is very difficult to follow the evolution of each sequence without overlapping effects between events. For this reason, the 2009 L'Aquila seismic sequence provides a clearer case-study for monitoring spatial and temporal changes of seismic attenuation before, during and after the main fault rupture. For this purpose, we select in this study earthquakes with accurate location and magnitude ($M_w \geq 3.2$) within a radius of 20 km from the main event to have better control of the temporal variation of the regional and near-source attenuation.

Because *S* waves attenuate significantly with the presence of fluids (Winkler & Nur 1982), we investigate in this paper whether the temporal and spatial variability of the spectral decay parameter κ

(Anderson & Hough 1984) may correlate with fluid flow in the epicentral area of the 2009 L'Aquila earthquake sequence. In addition, we also investigate the spatial and temporal variability of *S*-wave attenuation regionally and near the sources before, during and after the main rupture.

DATA

The data set used consists of 104 earthquakes with magnitude $M_L \geq 3.2$, in a radius of 20 km from the main event (as the rupture length), hypocentre distance $r < 170$ km and recorded by at least three stations. We estimated 2011 values of κ and formed four groups, 10 days before, during and 10 days and 6 months after the main event of 6 April 2009. Unlike an earlier study (Castro *et al.* 2022b), we selected events located near the epicentre of the main earthquake of the sequence to have a consistent volume sampled by the source–station *S*-wave paths. The hypocentre coordinates were taken from the seismic catalog of the Istituto Nazionale di Geofisica e Vulcanologia (INGV). The average location error reported in the INGV catalogue is less than one km.

The maps in Fig. 1 show the distribution of the seismic stations and the location of the main M_w 6.1 earthquake (red star), the foreshocks that occurred 10 days before (white dots), and aftershocks that occurred 10 days after (black dots). Most of the events have normal fault mechanisms and occurred along the active normal faults system in the Central Italy region. The stations are part of the Italian National Seismic Network (Rete Sismica Nazionale, RSN), which is operated by the Istituto Nazionale di Geofisica e Vulcanologia (INGV 2006), and the National Accelerometric Network (Rete Accelerometrica Nazionale, RAN, DPC 1972), that is managed by the Italian Civil Protection Department.

We selected records with signal-to-noise ratio (SNR) greater than three from earthquakes recorded by at least three stations. The records are sampled at 100 samples per second, baseline corrected and processed following the procedure described in Pacor *et al.* (2016) and Castro *et al.* (2022b). To determine the SNR, we select noise windows before the *P*-wave arrival having the same length as the *S*-wave signal. When events occurring close in time are recorded, the SNR before the *P*-wave arrival is typically less than three and the recording is rejected.

Fig. 2 displays the magnitude versus hypocentre distance of the data set. The local magnitudes of the earthquakes span from 3.2 to 5.9 and the recording distances from 4 to 170 km. Most events have a hypocentre distance between 9 and 100 km and focal depths between 6.5 and 17 km.

The estimates of κ can be affected by site amplifications when they occur at high frequencies (Ktenidou *et al.* 2013, 2014) and within the bandwidth used to measure κ (Perron *et al.* 2017). However, site effects will not affect the estimates of κ when site resonances are at lower frequencies than the band used to determine κ (Parolai & Bindi 2004). In this study, most of the recording stations used to measure κ are on class B sites ($V_{S\_30} = 360$–800 m s^{-1}), according to EC8 site classification, and have a natural frequency of resonance between 3 and 6.7 Hz. The frequency band selected to calculate κ is in the range of 8–38 Hz and the earthquakes have corner frequencies lower than 8 Hz. This frequency band was chosen to be above the corner frequency of the earthquakes analysed and below the frequency where signal to noise ratio is less than three, to avoid contamination from source dimension and near-site noise. For some of the stations a visual inspection was also carried out to verify the reliability of the band used.

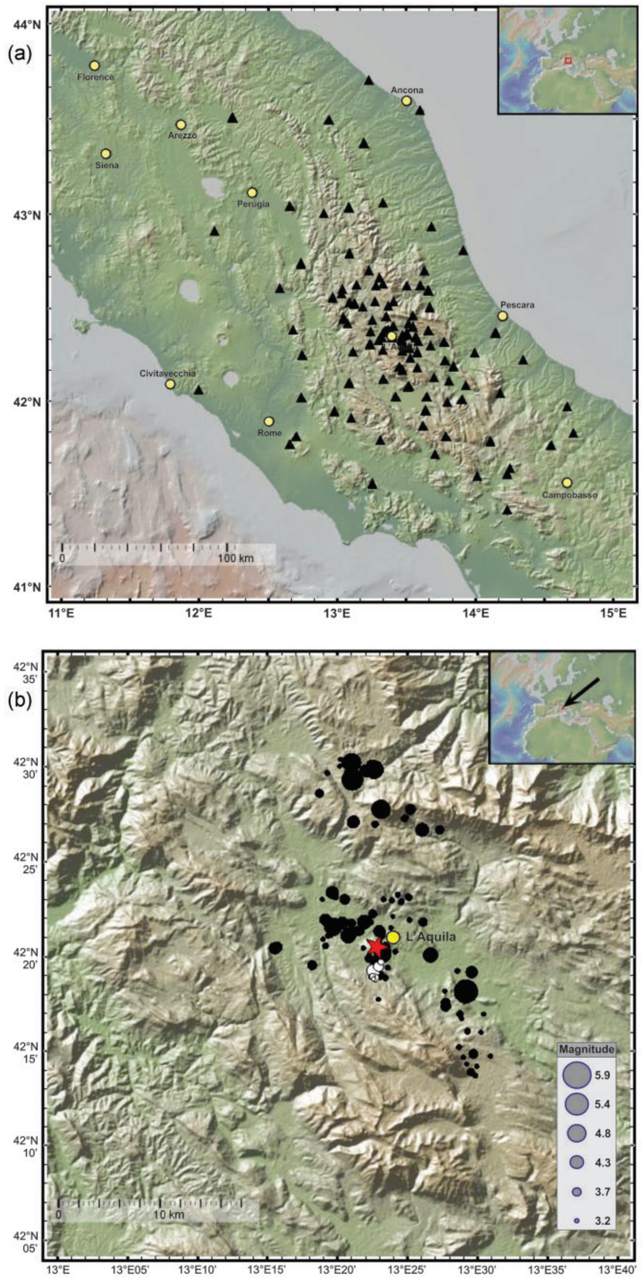

Figure 1. (a) Distribution of strong motion stations of the Central Italy array (triangles) and main cities (yellow circles) affected by the 6 April 2009, L'Aquila earthquake (M_w 6.1). (b) Location of the epicentres of the main event (red star), the foreshocks (white circles) and the aftershocks that occurred 10 days and 6 months (black circles) after the principal event.

METHOD

The parameter κ is like the attenuated traveltime $t*$ (Singh *et al.* 1982; Scherbaum 1990) and measures the average attenuation along the source–station path but may be also related with attenuation near the source and the recording site. This parameter controls the high frequency amplitude decay and uses the Brune (1970) model as source reference.

We estimated κ by least-squares fitting the *S*-wave high-frequency spectral amplitude acceleration as introduced by Anderson & Hough (1984):

$$A(f) = A_0\, e^{-\pi f \kappa}, \tag{1}$$

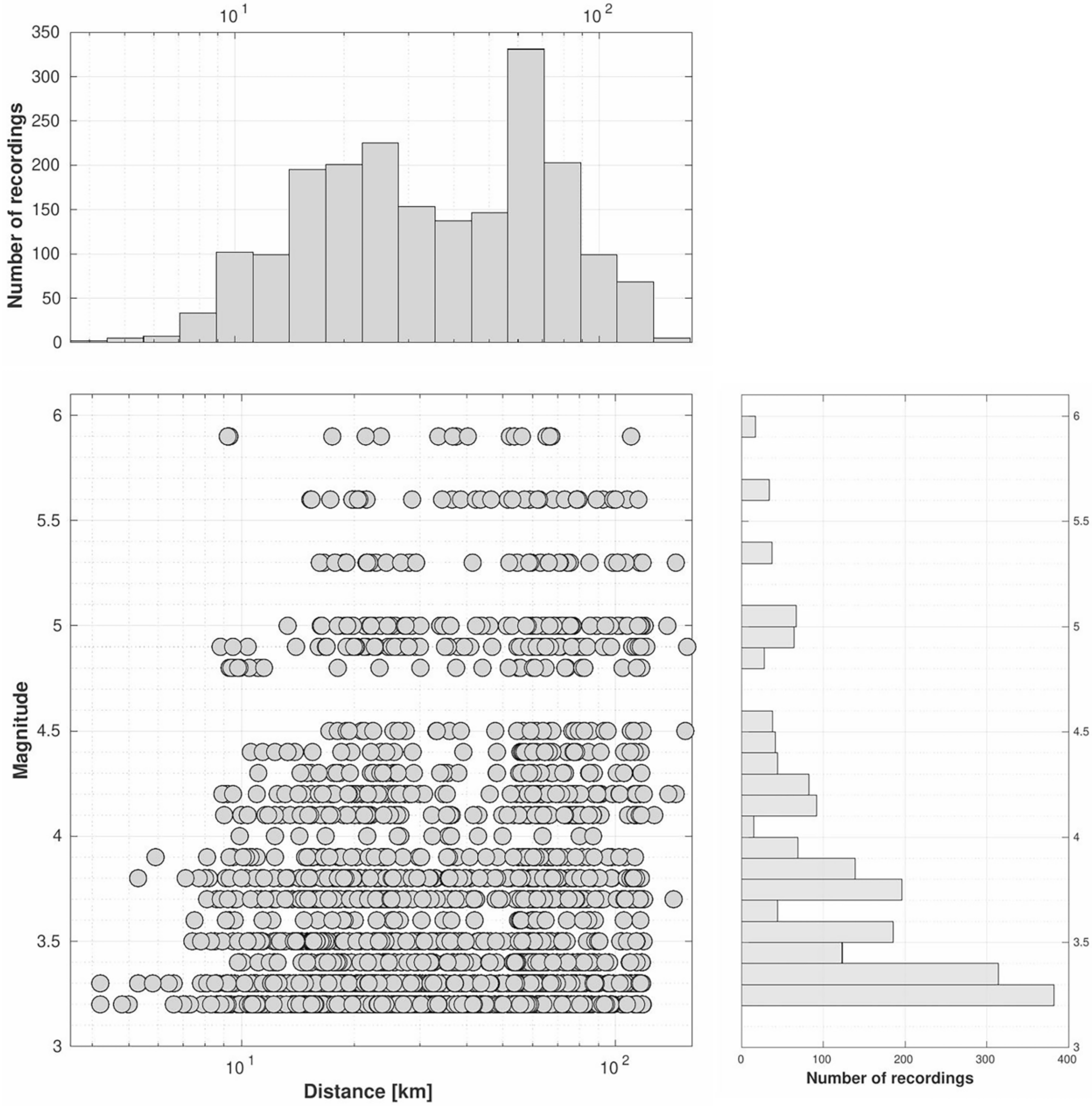

Figure 2. Number of recordings and earthquake magnitude (M_L) distribution with distance of the data set analysed. On top is the number of recordings and on the bottom is the magnitude distribution.

where $A(f)$ is the acceleration spectrum, A_0 depends on recording distance, source properties and other effects. To estimate κ eq. (1) is linearized by taking the logarithm on both sides of the equation.

Fig. 3 displays an example of acceleration spectra plotted on a semi-log scale from an earthquake magnitude $M = 3.8$ recorded at 31.3 km at station LSS. κ is estimated with the slope of the least-squares fit of the spectral amplitudes, $\kappa = -slope/\pi\, Log(e)$.

Because of the large number of records, we used a semi-automatic technique that calculates for each individual record the slopes over 11 frequency bands with length varying between 8 and 38 Hz (Lanzano *et al.* 2022) to estimate the median value of κ and the standard deviation. This technique has been used and discussed in more detail in previous studies (Castro *et al.* 2022a,b).

Fig. 4 shows the values of κ calculated with this technique using records from foreshocks (left-hand panel), the L'Aquila main event (centre panel) and the aftershocks (right-hand panel). The apparent scatter of the measured κ is due to different attenuation contributions near the recording sites and the sources, nevertheless, it is evident that κ tends to increase with hypocentre distance.

The estimated values of κ were modelled as in Anderson (1991), Ktenidou *et al.* (2014) and Castro *et al.* (2022a):

$$\kappa\,(\kappa_s, r, \kappa_0) = \kappa_s + \tilde{\kappa}\,(r) + \kappa_0, \tag{2}$$

where κ_s is the near-source attenuation, $\tilde{\kappa}(r)$ is the regional average attenuation along the S-wave source–station distance r and κ_0 is the near-site attenuation. Van Houtte *et al.* (2011) introduced

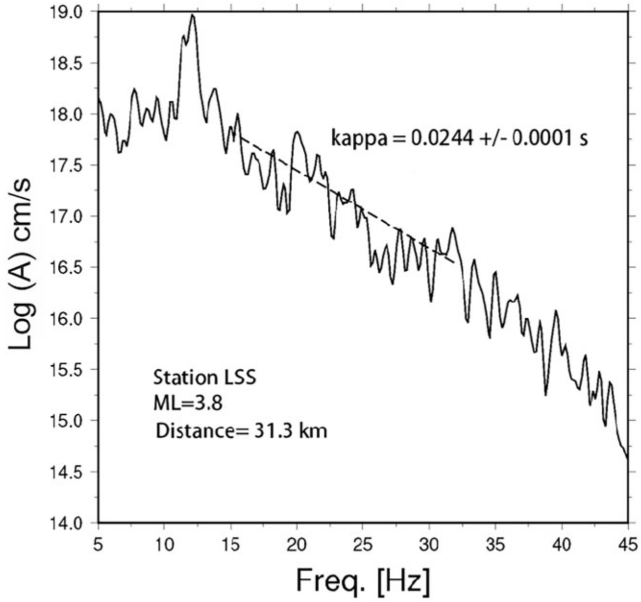

Figure 3. Acceleration spectra from an $M = 3.8$ recorded at 31.3 km at station LSS. The slope of the dashed line is proportional to the estimated value of κ of 0.0244 s.

an inversion technique to separate simultaneously source, site and path contributions to κ, which is like the method proposed by Oth *et al.* (2011) for the Generalized spectral Inversion Technique (GIT). However, for this investigation we prefer to use a two-step approach, as in Castro *et al.* (2022b), to estimate these contributions to minimize the trade-off between κ_s and $\tilde{\kappa}(r)$, and to improve the resolution.

We calculated first the regional average attenuation $\tilde{\kappa}(r)$ with the non-parametric technique. For that purpose, eq. (2) can be rewritten as:

$$\kappa(r) = \kappa_1 + \tilde{\kappa}(r), \tag{3}$$

where κ_1 includes both κ_s and κ_0. To solve eq. (3), we assume that $\tilde{\kappa}(r)$ is a smooth function of r, that κ varies slowly with distance, that $\tilde{\kappa}(0) = 0$, and that the shape of $\tilde{\kappa}(r)$ is the same for all the earthquakes considered, so that undulations in the observed κ are related to κ_1.

We estimate κ_1 in a second iteration by correcting the observed values of κ with the function $\tilde{\kappa}(r)$ obtained solving eq. (3). Then, we resolve the remaining system of equations as in Castro *et al.* (2022b):

$$\kappa_{1ij} = \kappa_{0i} + \kappa_{sj}, \tag{4}$$

where κ_{1ij} is the corrected value, using $\tilde{\kappa}(r)$, of the observed κ from site i and source j; κ_{0i} is the near-site attenuation parameter at station i and κ_{sj} is the near-source attenuation from earthquake j. To resolve the degree of freedom between κ_{0i} and κ_{sj}, we constrained eq. (4) to satisfy the condition:

$$\sum_{i=1}^{N} \kappa_{0i} = 0, \tag{5}$$

where N is the number of reference sites used for that constraint. We used two reference sites having the smallest near-site attenuation ($\kappa_0 < 0.0296$ s). Eq. (5) conditions the reference sites to have a null near-site attenuation effect in the inversion.

RESULTS AND DISCUSSION

Regional average *S*-wave attenuation

Fig. 5 shows average regional $\tilde{\kappa}(r)$ functions obtained using records from foreshocks (plusses) 10 days before the main shock, and aftershocks that occurred 10 days (stars) and 6 months (crosses) after the principal event (green circles). For the foreshocks, $\tilde{\kappa}(r)$ takes values less than 0.0170 s with an error of 0.0081 s and for the aftershock the values of $\tilde{\kappa}(r)$ are less than 0.0760 s with an error of 0.0108 s. The error bars in Fig. 5 represent the deviation of the measured κ values with respect to the regional mean.

Because the spectral decay parameter is inversely proportional to the quality factor Q and this attenuation parameter depends on the physical characteristics of the crustal rocks, such as the presence of fluids and the pressure generated by tectonic stress, the temporal variation of $\tilde{\kappa}(r)$ can be interpreted in terms of these physical parameters. When rocks are fluid saturated Q tends to be low and S waves attenuate significantly (Johnston *et al.* 1979; Toksoz *et al.* 1979). On the other hand, when rocks are under high pressure Q is high and S waves attenuate less, as shown in laboratory rock experiments (Tisato & Quintal 2014; King *et al.* 2022).

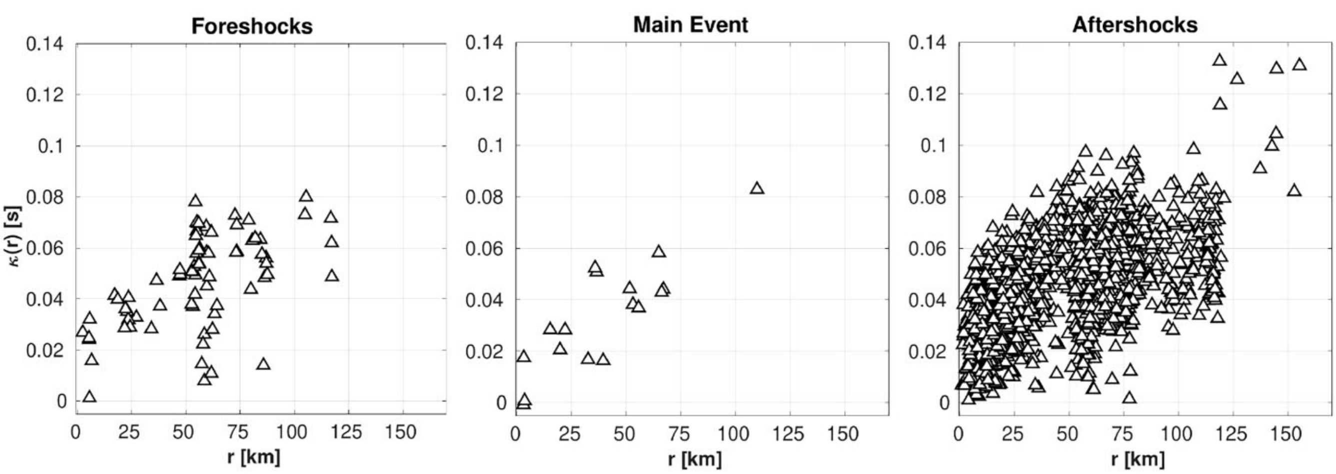

Figure 4. Estimates of the spectral decay parameter kappa (κ) obtained using records from the foreshocks (left-hand panel), the main event (centre panel) and the aftershocks (right-hand panel).

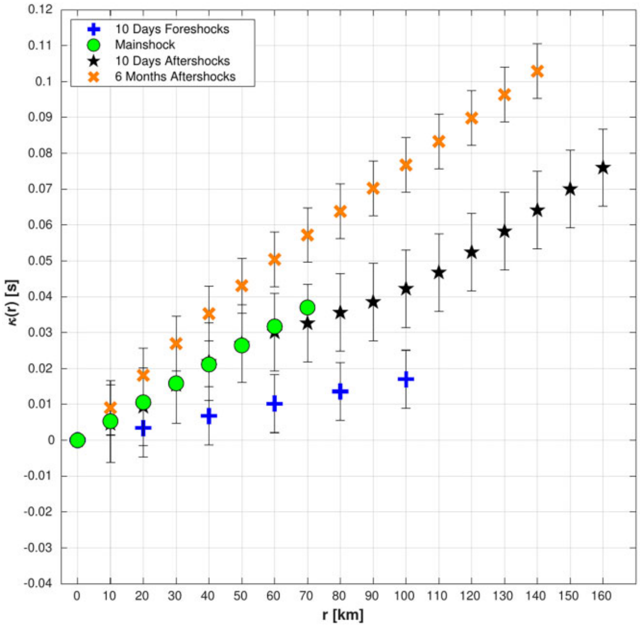

Figure 5. Temporal variation of the average regional kappa $\tilde{\kappa}(r)$ along the source–station paths calculated using foreshocks that occurred 10 days before the main event (blue plus), during the main shock (green circles), using aftershocks that occurred ten days after (black stars) and 6 months after (orange crosses). The bars on the values of $\tilde{\kappa}(r)$ represent the uncertainty of the estimate.

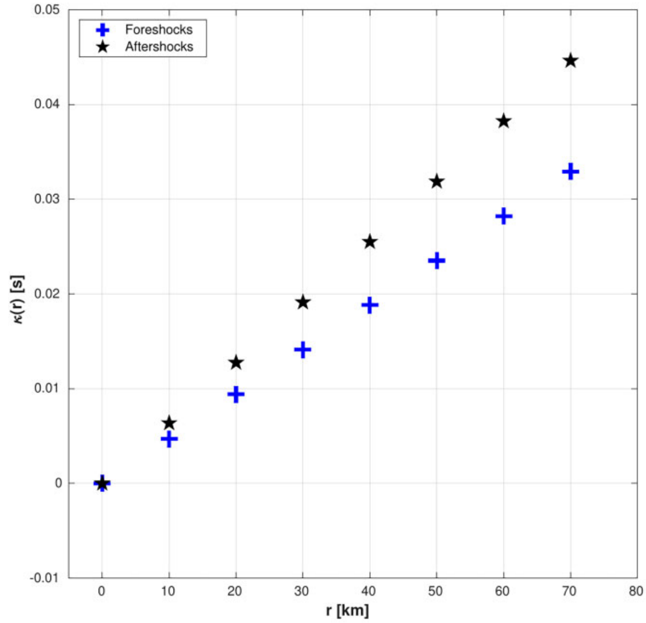

Figure 6. Average regional $\tilde{\kappa}(r)$ along source–station paths calculated using a foreshock occurred on 30 March 2009 (crosses) and an aftershock on 6 April 2009 (stars) with the same epicentral location and registered at the same stations.

Fig. 5 shows that 10 days before the L'Aquila main shock the high frequency *S*-wave attenuation was low outside the rupture area (r > 20 km), presumably when the regional tectonic stress was high. Borghi *et al.* (2016) calculated Coulomb failure stresses and found stress changes in the epicentral area of the main rupture that increased between 0.11 and 0.20 MPa. Then, during the main rupture (green circles), the attenuation increased because the stress dropped during the fault rupture. Malagnini *et al.* (2012) estimated strength reductions of 7–10 MPa during the fault rupture process. During the 10-day aftershock sequence $\tilde{\kappa}(r)$ did not change much because in this short time interval the regional tectonic stress probably did not change much. The productivity of aftershocks is influenced by several factors such as fault dimensions, lithospheric age and stress drop (Dascher-Cousineau *et al.* 2020). Calderoni *et al.* (2019) did not observe significant stress-drop differences between the main shock and the aftershocks, which indicates that the average tectonic stress did not change much during the 10 days after the main shock, and the average *S*-wave regional attenuation remain the same, as shown in Fig. 5. Lolli *et al.* (2011) analysed the statistics of the L'Aquila aftershock sequence and found that in the first 2 weeks after the main shock the aftershock rate decreased as predicted by Omori's law (Omori 1894).

Six months after the main event the attenuation in the epicentral region was higher because the tectonic stress accumulated was mostly released and a new earthquake cycle probably started.

To verify the validity of the method and the results, we selected one foreshock and one aftershock with the same location (Table 1) and recorded by the same stations to calculate the average regional kappa $\tilde{\kappa}(r)$, before and after the main shock. The distance between these two events is 0.54 km, they have the same focal depth and approximately the same magnitude (Table 1). Fig. 6 shows that before the main shock the values of $\tilde{\kappa}(r)$ were less than during the aftershock, in consistency with Fig. 5.

Two additional sensitivity tests were made to prove that we separated well spatial from temporal changes of $\tilde{\kappa}(r)$: (1) we calculated $\tilde{\kappa}(r)$ selecting all foreshocks (10 days before the main shock) and aftershocks (10 days after), from our dataset, that intersected the same crustal volume (Fig. 7) and that were recorded at the same stations. The magnitudes of these earthquakes vary between 3.2 and 4.8, have focal depths 9.2–10.9 km and are located within a radius of about 3 km from the main shock. (2) We estimated $\tilde{\kappa}(r)$ considering aftershocks 10 days after the main shock and located outside of the foreshocks and main shock volume (Fig. 8). Note that this second volume samples the north side of the main rupture. The average regional kappa obtained for these two crustal volumes is displayed in Fig. 9. In the first volume $\tilde{\kappa}(r)$ during the foreshocks is lower than during the aftershocks as in Fig. 5. In contrast, $\tilde{\kappa}(r)$ calculated with the aftershocks that sampled the second crustal volume, outside the foreshock–main shock volume, shows the same low attenuation values than the foreshocks, suggesting that a considerable amount of stress was transferred outside the foreshock–main shock volume and that the crustal Q increased. The significant difference of $\tilde{\kappa}(r)$ between the two volumes sampled by the aftershocks also indicates that there was a spatial variation of the average regional attenuation during the same period (10 days after the main shock).

Table 1. Earthquakes selected to calculate the average regional kappa (see Fig. 6).

Event	Date	Time	M	Latitude N	Longitude E	H (km)
Foreshock	2009-03-30	13:43:26	3.6	42°18.90′	13°22.68′	9.7
Aftershock	2009-04-06	10:12:35	3.7	42°19.02′	13°23.04′	9.7

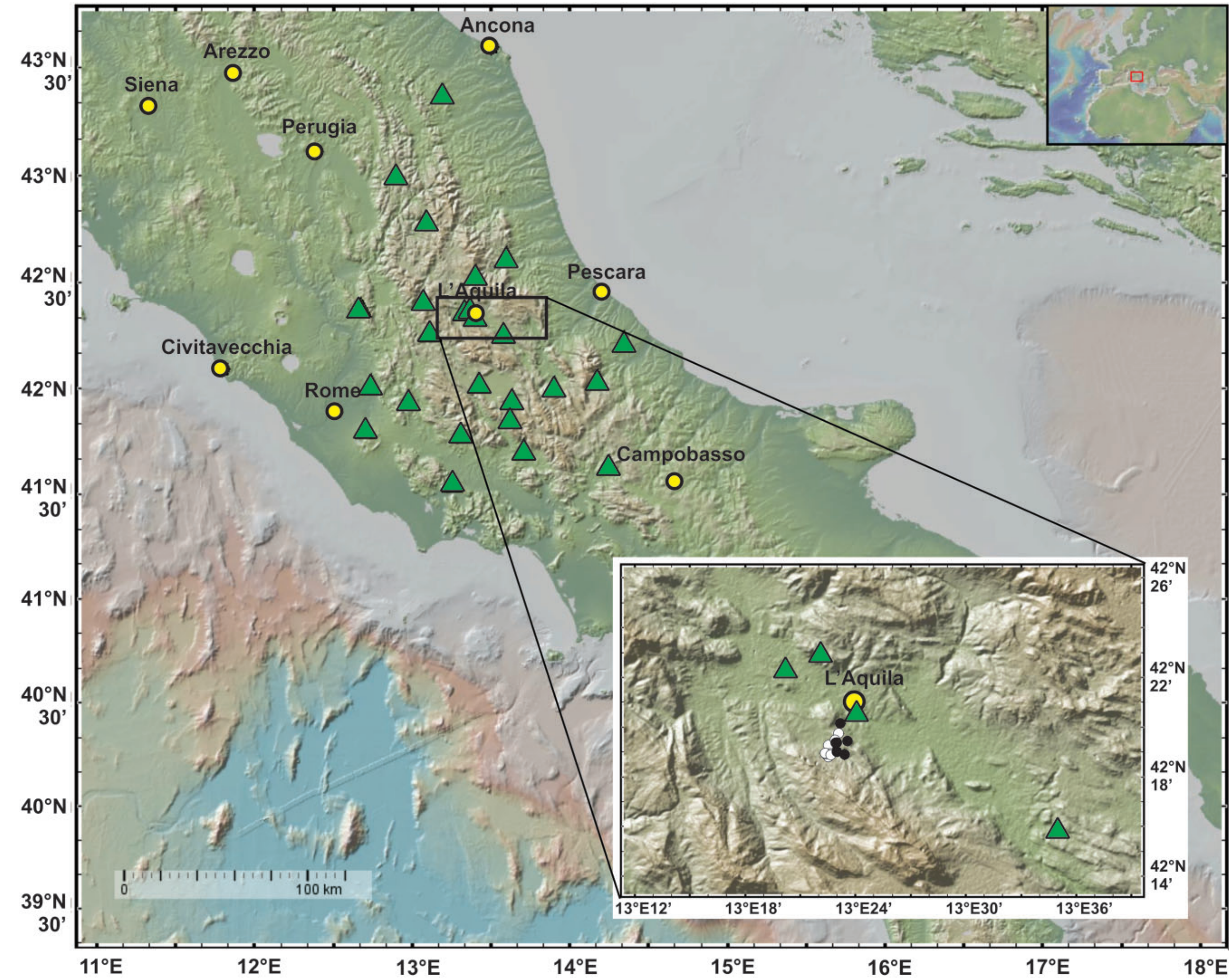

Figure 7. The location of foreshocks (white circles) and aftershocks (black circles) that occurred 10 days before and after the main shock, respectively, intersecting the same volume (lat: 42.314–42.329; lon: 13.373–13.385). The triangles are the stations that recorded these earthquakes.

To analyse how the difference in data population before and after the main shock (Fig. 4) could affect the estimates of the average regional attenuation, we compare the estimates of $\tilde{\kappa}(r)$ from the aftershocks displayed in Fig. 5 with those in Fig. 9 (Table 2). Note that the number of aftershocks used to calculate $\tilde{\kappa}(r)$ in Fig. 5 is greater than those in Fig. 9 but both groups of aftershocks sample the same crustal volume. The difference in the estimates of $\tilde{\kappa}(r)$ vary between 2 and 18%, depending on the distance range (Table 2). Therefore, the difference in number of earthquakes used to estimate $\tilde{\kappa}(r)$ before and after the main shock (Fig. 5) will not generate a bias greater than 18%. The main reason is that both datasets cluster in a small volume and the dense distribution of stations is similar.

Near-source attenuation (κ_s)

The map in Fig. 10 shows the location of the main earthquake (white star) and the distribution of foreshocks with $M \geq 3.2$ in a radius of 20 km from the main shock. The different colours represent different values of κ_s, blue ($\kappa_s \sim 0.0$), green ($\kappa_s \sim 0.0038$ s) representing low *S*-wave attenuation and pink ($\kappa_s \sim 0.0150$ s) and white ($\kappa_s = 0.0280$ s) high attenuation. Note that κ_s increased by at least a factor between 2 and 7 near the main source compared with the near-source attenuation of the foreshocks. It is likely that tectonic stress was high southwest of the main shock epicentre, where κ_s was low and perhaps crustal fluids flowed northeast towards the main event where the density of the fractures and the porosity of the rocks was higher. It is interesting to note that κ_s was very high where the main rupture started (white star), indicating the likely presence of crustal fluids which perhaps lubricated the fault and initiated the rupture. This result agrees with an independent investigation of Lucente *et al.* (2010) who analysed the temporal variation of seismic velocity before the main event of the L'Aquila sequence and found that migration of crustal fluids was connected to the preparatory phase of the M_w 6.1 main shock.

Di Luccio *et al.* (2010) observed an increase of the V_P/V_S ratio from October 2008 to 6 April 2009, when the main event occurred, due to increasing pore fluid pressure along the faults. They estimated values of V_P/V_S between 1.83 and 1.95 for the foreshock–aftershock L'Aquila sequence, which are consistent for fluid-rich rocks (Zhao & Negishi 1998). Di Luccio *et al.* (2010) calculated a hydraulic diffusivity of 80 m^2 s^{-1} and a permeability of approximately 10^{-12} m^2 suggesting the presence of CO_2-rich fluids within a fractured medium. The importance of fluids content in seismic sequences is

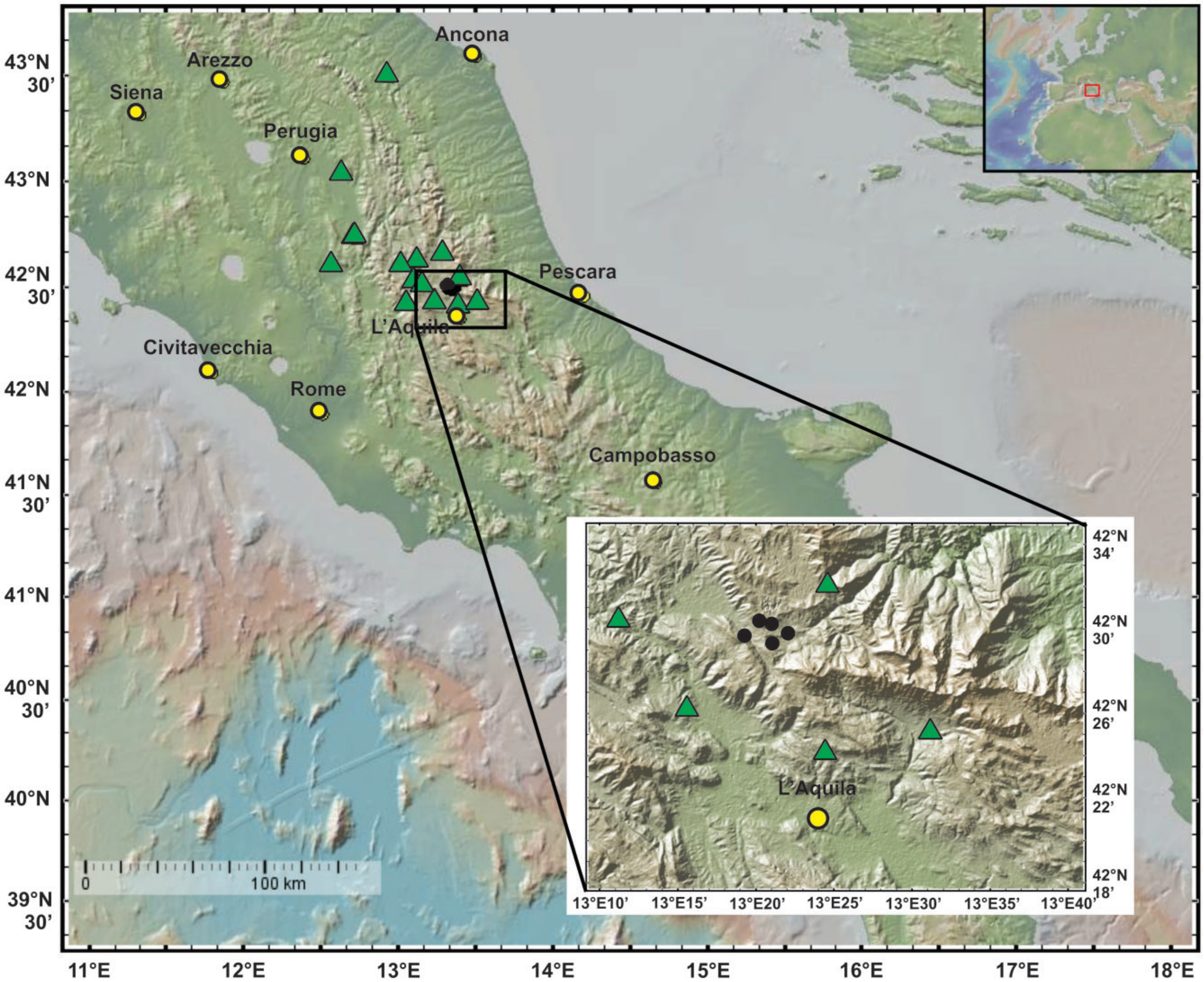

Figure 8. The location of the aftershocks (black circles) that occurred 10 days after the main shock within a volume outside the foreshock and main shock volume (lat: 42.483–42.517; lon: 13.325–13.367). The triangles are the stations that recorded these earthquakes and that were used to calculate $\tilde{\kappa}(r)$.

also suggested by Sibson (2009) who found that the L'Aquila main shock was anticipated by hydrofracturing dilatancy and by Picozzi *et al.* (2022a) who found that the foreshocks are characterized by a progressive increase in slip per unit stress. Fig. 10 (on the right) also shows an increase of κ_s with depth between 9.5 and 10 km, below the focal depth of the main earthquake. Borghi *et al.* (2016) reported a M_w 5.9 slow-slip event (SSE) that occurred approximately 2 months before the main fault rupture, beneath the normal fault system of Paganica that generated the L'Aquila seismic sequence. The decollement that originated the SSE is located around 9 km depth, it had the largest slip of 2 cm over an area of 160 km^2 and it is plausible that the SSE generated significant stress to trigger the main foreshocks that favour a fluid diffusion process that initiated the rupture process of the L'Aquila main earthquake (Borghi *et al.* 2016). Previous studies have suggested that the seismotectonic of Central Italy is related with uprising of fluids from the mantle (Ghisetti & Vezzani 2002; Chiodini *et al.* 2004) and the more recent study by Di Luccio *et al.* (2010) concluded that upward migration of fluids generated an increase of pore pressure in cracks and rock pores. These observations are consistent with the spatial distribution of the foreshocks and their high values of κ_s shown in Fig. 10.

The number of aftershocks with $M \geq 3.2$ that occurred 10 days after the main shock (Fig. 11) increased considerably and most of them show moderate ($0.004 < \kappa_s < 0.010$ s) to high attenuation ($\kappa_s < 0.0209$ s) near the source, particularly near the epicentre of the main event and those located north and southeast, suggesting that the fluids remained in the epicentral area at least for 10 days after the main shock. Three larger earthquakes ($M > 4.9$) occurred north of the main shock epicentre, during the first 4 days after, that Malagnini *et al.* (2012) suggested were induced by a reduction of shear strength due to a pulse of pore fluid pressure generated after the main event. Aftershocks located farther north, at the mountain ranges, show lower values of κ_s, suggesting less fluid saturated rocks. These observations are consistent with Malagnini *et al.* (2012) study that shows a fluid migration process in the N–NW direction from the main hypocentre, and the activation of the Campotosto fault that seems to be modulated by a diffusion process. In the SE direction from the main hypocentre, no further ruptures on adjacent structures were triggered, and the entire volume around the Paganica fault was activated almost instantaneously at the occurrence of the main shock. This may explain why we observe more attenuation towards this sector, which is characterized by higher κ_s values with respect to the surroundings.

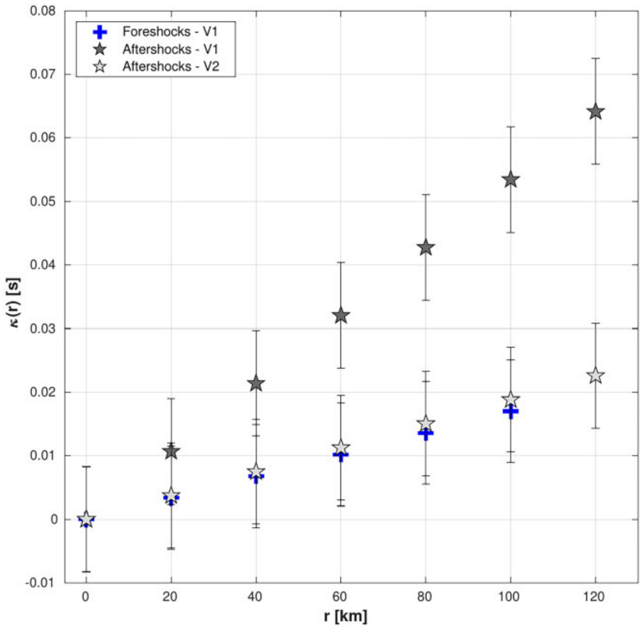

Figure 9. Average regional $\widetilde{\kappa}(r)$ along source–station paths calculated using foreshocks (plus) and aftershocks (black stars) intercecting the same volume 1 (Fig.7), and using aftershocks (gray stars) in volume 2 (Fig. 8).

Table 2. Estimates of the average regional attenuation $\tilde{\kappa}(r)$ using aftershocks 10 days after the main shock that sample the same respective crustal volume. The volume 1 corresponds to estimates of $\tilde{\kappa}(r)$ displayed in Fig. 9. Note that the number of aftershocks used for volume 1 is similar to the foreshocks in Fig. 5.

r (km)	$\tilde{\kappa}(r)$ (volume 1)	$\tilde{\kappa}(r)$ Fig. 5	Per cent changed
20.0	0.01 069	0.00 935	12.5
40.0	0.02 138	0.02 187	2.2
60.0	0.03 206	0.03 012	6.1
80.0	0.04 275	0.03 560	16.7
100.0	0.05 344	0.04 224	21.0
120.0	0.06 413	0.05 242	18.3

The near-source κ_s can also give us some idea of the depths where rocks are more fluid saturated. Figs 10 and 11 display the focal depths of the 10-day foreshock and aftershock seismic sequence, respectively, versus κ_s. The depths of the hypocentres have a location error of less than 10%, as in Castro *et al.* (2022b). For the foreshocks κ_s takes values less than 0.0155 s with errors between 0.0072 and 0.0075 s, and for the aftershocks κ_s is less than 0.0209 s with errors varying between 0.0081 and 0.0089 s. Most aftershocks have focal depths between 8 and 12 km, about the depth of the main event hypocentre (8.3 km). The foreshocks are the deepest of the sequence, with greater focal depth than the main event, with focal depths between 9.2 and 10 km. They also show an increase of κ_s towards the main event, suggesting a possible presence of crustal fluids in that direction and towards the surface. This trend is also consistent with the map of temporal evolution of the energy index (*EI*) obtained by Picozzi *et al.* (2022b) which shows an area south of the main shock epicentre with low *EI* values. The *EI* is defined as the difference between the seismic energy *Es* observed and the values associated with the median scaled energy *Es/Mo* which is related to the apparent stress and the seismic efficiency. Picozzi *et al.* (2022b) found that when the activation phase starts there is a decrease of EI below 1.5 MPa. Note on Fig. 10 that the main event (plotted with a star) has shallower depth and a higher value of κ_s than the foreshocks, suggesting that the rocks near the rupture of the main event were probably more fluid saturated. The foreshock study by Lucente *et al.* (2010) indicates that an over-pressurized zone in the crust was located below the nucleation area of the L'Aquila main earthquake and therefore the aftershocks were probably induced by a reduction in the fault's shear strength, as observed by Malagnini *et al.* (2012). Ten days after the main shock (Fig. 11) most aftershocks are between 7 and 11 km deep, where the seismogenic zone is presumably located and where the main earthquakes nucleate in Central Italy.

CONCLUSIONS

The quality and quantity of the seismic records used permit us to detected spatial-temporal variations of *S*-wave attenuation in the epicentral area of the L'Aquila earthquake sequence of 2009 using the spectral decay parameter κ (Anderson & Hough 1984) which is sensitive to the fluid migration and may serve as a forecasting proxy for fluid-driven earthquake triggering. We separated the average regional attenuation, and the near-source and near-site contributions of κ and found that the lowest regional attenuation $\widetilde{\kappa}(r)$ observed 10 days before the main shock may be the result of high tectonic stress accumulated near the epicentral area.

We found that the temporal variation of κ is consistent with changes of the V_P/V_S ratio, reported in previous studies, during the foreshock sequence and with the variation of the fracture field properties with time, as demonstrated in Nur (1972) and Scholz *et al.* (1973). In agreement with previous studies by Lucente *et al.* (2010) and Di Luccio *et al.* (2010), variations of fluid pressure conditions can cause large scatter which may explain the spatial variability of κ_s observed in our study.

During the main shock $\tilde{\kappa}(r)$ increased because the stress dropped during the rupture process, when strength reductions of 7–10 MPa occurred (Malagnini *et al.* 2012). The aftershocks that occurred 6 months after show an increase in the regional attenuation probably due to the reduced tectonic stress in the epicentre region caused by the stress released during the main shock and the earlier aftershocks. The observed increased values of the near-source attenuation κ_s near the hypocentre of the main shock suggests the presence of crustal fluids in the rupture zone. The observed spatial variation of κ_s of the foreshocks indicates that the fluids flowed towards the rupture area from below before the rupture of the main event initiated.

We conclude that investigations of κ can provide important clues for the monitoring of the earthquake cycle in Central Italy, and that the integration of other parameters, like the radiated seismic energy (Picozzi *et al.* 2023), and the V_P/V_S ratio together with κ may be also useful to study the preparatory phases of future earthquakes. Moreover, the estimates of κ can be fully automated and implemented in regions that are prone to earthquakes and have an adequate station coverage.

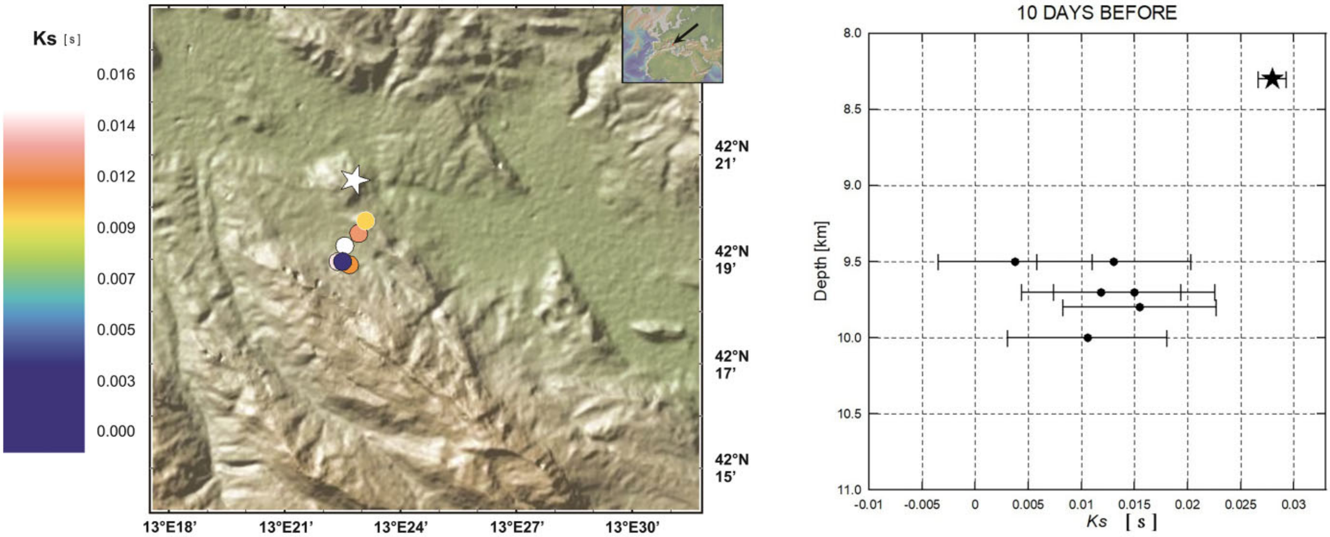

Figure 10. Estimates of near-source kappa (κ_s) values using foreshocks that occurred 10 days before the main shock (star). Note in the right frame that the foreshocks are below the main event and that there is an increase of attenuation towards the L'Aquila earthquake (M_{w} 6.1), suggesting possible migration of crustal fluids in that direction. The bars on the values of κ_s (right frame) represent the uncertainty of the estimate.

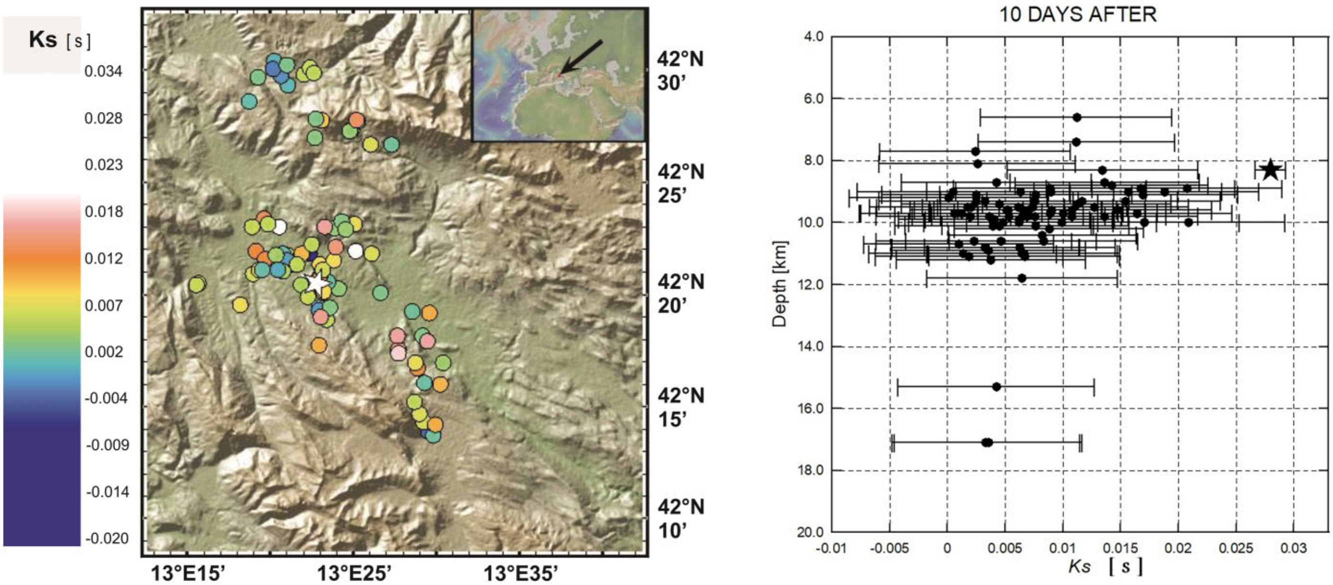

Figure 11. Near-source κ_s values estimated using aftershocks that occurred 10 days after the main shock (star). Note that the main shock and most aftershocks have similar focal depths, lower attenuation concentrates at the northwestern end of the epicentral area and higher attenuation at the southeastern zone.

ACKNOWLEDGMENTS

This research was supported by INGV in the frame of the project '*Pianeta Dinamico*' project—SECURE (Regional-Scale Earthquake Ground Motion Predictions Through Physics-based and Empirical Approaches: A Case study Central Italy), funded by MIUR (Italian Ministry of University and Research) aimed at the relaunch of investments of the central administrations of the State and development of the country). I thank the technical support of Antonio Mendoza Camberos, Euclides Ruiz Cruz and Arturo Pérez Vertti from the Earth Science Division, Department of Seismology of CICESE. Comments and suggestions provided by Prof Yehuda Ben-Zion are also appreciated. The authors are grateful to the Editor Dr Sidao Ni, two anonymous reviewers and Prof Luca De Siena for their comments and suggestions that improve this paper.

AUTHOR CONTRIBUTIONS

The results of this paper were analysed by R. Castro, L. Colavitti, F. Pacor, G. Lanzano and S. Sgobba. The data was processed by D. Spallarossa, R. Castro and L. Colavitti. The paper was written by R. Castro and L. Colavitti.

DATA AVAILABILITY

The data used comes from permanent networks operated by the INGV (Istituto Nazionale di Geofisica e Vulcanologia): the National Seismic Network (RSN) and the Mediterranean Network (Mednet); the Rapid Response Networks that are operated together with the University of Genoa and the RESIF (*Réseau Seismologique et Géodésique Français*). Other permanent stations belong to the

National Accelerometric Network (RAN), operated by the Department of Civil Protection. The acceleration records can be obtained from the Italian Accelerometric Archive (http://itaca.mi.ingv.it), and the velocity records from the European Integrated Data Archive (EIDA; http://eida.rm.ingv.it). Some plots were made using Generic Mapping Tools (http://www.soest.hawaii.edu/gmt; Wessel & Smith 1998), and with GeoMapApp (http://www.geomapapp.org).

REFERENCES

Ameri, G., Gallovič, F. & Pacor, F. 2012. Complexity of the Mw 6.3 2009 L'Aquila (Central Italy) earthquake: 2. Broadband strong-motion modeling, *J. geophys. Res.,* **117**(B4), doi:10.1029/2011JB008729.

Anderson, J.G. & Hough, S.E., 1984. A model for the shape of the Fourier amplitude spectrum of acceleration at high frequencies, *Bull. seism. Soc. Am.,* **74,** 1969–1984.

Anderson, J.G. 1991. A preliminary descriptive model for the distance dependence of the spectral decay parameter in southern California, *Bull. seism. Soc. Am.,* **81,** 2186–2193.

Beroza, G.C., Cole, A.T. & Ellsworth, W.L., 1995. Stability of coda wave attenuation during the Loma Prieta, California, earthquake sequence, *J. geophys. Res.,* **100**(B3), 3977–3987.

Bonilla, L.F. & Ben-Zion, Y., 2021. Detailed space-time variations of the seismic response of the shallow crust to small earthquakes from analysis of dense array data, *Geophys. J. Int.,* **225,** 298–310.

Borghi, A., Aoudia, A., Javed, F. & Barzaghi, R., 2016. Precursory slow-slip loaded the 2009 L'Aquila earthquake se quence, *Geophys. J. Int.,* **205,** 776–784.

Brune, J.N., 1970. Tectonic stress and the spectra of seismic shear waves from earthquakes, *J. geophys. Res.,* **75,** 4997–5009.

Cabrera, L., Poli, P. & Frank, W.B., 2022. Tracking the spatio-temporal evolution of foreshocks preceding the Mw 6.1 2009 L'Aquila earthquake, *J. geophys. Res.,* **127,** e2021JB023888, doi:10.1029/2021JB023888.

Calderoni, G., Rovelli, A. & Di Giovambattista, R., 2019. Stress drop, apparent stress, and radiation efficiency of clustered earthquakes in the nucleation volume of the 6 April 2009, Mw 6.1 L'Aquila earthquake, *J. geophys. Res.,* **124**(10), 360–375.

Calderoni, G., Rovelli, A., Ben-Zion, Y. & Y. Di Giovambattista, Y., 2015. Along-strike rupture directivity of eartquakes of the 2009 L'Aquila, central Italy, seismic sequence, *Geophys. J. Int.,* **2003,** 399–415.

Castro, R.R., Colavitti, L., Vidales-Basurto, C.A., Pacor, F., Sgobba, S. & Lanzano, G., 2022a. Near-source attenuation and spatial variability of the spectral decay parameter kappa in Central Italy, *Seismol. Res. Lett.,* **93**(4), 2299–2310.

Castro, R.R., Spallarossa, D., Pacor, F., Colavitti, L., Lanzano, G., Vidales-Basurto, C.A. & Sgobba, S., 2022b. Temporal variation of the spectral decay parameter kappa detected before and after the 2016 main earthquakes of central Italy, *Bull. seism. Soc. Am.,* **112,** 3037–3045.

Chiarabba, C. *et al.*, 2009. The 2009 L'Aquila (central Italy) MW6.3 earthquake: main shock and aftershocks, *Geophys. Res. Lett.,* **36**(18), doi:10.1029/2009GL039627.

Chiarabba, C., De Gori, P., Valoroso, L., Petitta, M. & Carminati, E., 2022. Large extensional earthquakes push-up terrfic amount of fluids, *Sci. Rep.,* **12,** 1–10.

Chiaraluce, L., Valoroso, L., Piccinini, D., Di Stefano, R. & De Gori, P., 2011. The anatomy of the 2009 L'Aquila normal fault system (central Italy) imaged by high resolution foreshock and aftershock locations, *J. geophys. Res.,* **116**(B12), doi:10.1029/2011JB008352.

Chioccarelli, E. & Iervolino, I., 2010. Near-source seismic demand and pulse-like records: a discussion for L'Aquila earthquake, *Earthq. Eng. Struct. Dyn.,* **39**(9), 1039–1062.

Chiodini, G., Cardellini, C., Amato, A., Boschi, E., Caliro, S., Frondini, F. & Ventura, G., 2004. Carbon dioxide earth degassing and seismogenesis in central and southern Italy, *Geophys. Res. Lett.,* **31**(7), doi:10.1029/2004GL019480.

Chouet, B., 1979. Temporal variation in the attenuation of earthquake coda near Stone Canyon, California, *Geophys. Res. Lett.,* **6,** 143–146.

D'Amico, S., Orecchio, B., Presti, D., Neri, G., Wu, W.-N., Sandu, I., Zhu, L. & Herrmann, R.B., 2013. Source parameters of small and moderate earthquakes in the area of the 2009 L'Aquila earthquake sequence (central Italy), *Phys. Chem. Earth,* **63,** 77–91.

Dascher-Cousineau, K., Brodsky, E.E., Lay, T. & Goebel, T., 2020. What controls variations in aftershock productivity?, *J. geophys. Res.,* **125,** doi:10.1029/2019JB018111.

Del Pezzo, E. & Zollo, A., 1984. Attenuation of coda waves and turbidity coefficient in central Italy, *Bull. seism. Soc. Am.,* **74,** 2655–2659.

Di Luccio, D., Ventura, G., Di Giovambattista, R., Piscini, A. & Cinti, F.R., 2010. Normal faults and thrusts reactivated by deep fluids: the 6 April 2009 Mw 6.3 L'Aquila earthquake, central Italy, *J. geophys. Res.,* **115**(B6), doi:10.1029/2009JB007190.

DPC, 1972. *Presidency of Council of Ministers—Civil Protection Department. Italian Strong Motion Network [data set]*. International Federation of Digital Seismograph Networks. https://doi.org/10.7914/SN/IT.

Falcucci, E. *et al.*, 2009. The Paganica fault and surface coseismic ruptures caused by the 6 April 2009 earthquake (L'Aquila, central Italy), *Seismol. Res. Lett.,* **80**(6), 940–950.

Fonzetti, R., Valoroso, L., De Gori, P. & Chiarabba, C., 2024. Localization of deformation on faults driven by fluids during the L'Aquila 2009 earthquake, *J. geophys. Res.,* **129,** doi:10.1029/2024JB029075.

Gabrielli, S., Akinci, A., De Siena, L., Del Pezzo, E., Buttinelli, M., Maesano, F.E. & Maffucci, R., 2023. Scattering attenuation images of the control of thrusts and fluid overpressure on the 2016–2017 Central Italy seismic sequence, *Geophys. Res. Lett.,* **50,** e2023GL103132, doi:10.1029/2023GL103132.

Gallovič, F. & Zahradník, J., 2012. Complexity of the Mw6.3 2009 L'Aquila (Central Italy) earthquake: 1. Multiple finite-extent source inversion, *J. geophys. Res.,* **117**(B4), doi:10.1029/2011JB008709.

Ghisetti, F. & Vezzani, L., 2002, Normal faulting, transcrustal permeability and seismogenesis in the Apennines (Italy), *Tectonophysics,* **348,** 155–168.

Gholamzadeh, A., Rahimi, H. & Yaminifard, F., 2013. Spatial and temporal variation of coda-wave attenuation in the Faryab region, southern of the Sanandai-Sirjan zone, using aftershocks of the Tiab earthquake of 28 February 2006, *Bull. seism. Soc. Am.,* **104**(1), 529–539.

Got, J.L., Poupinet, G. & Frechet, J., 1990. Changes in source and site effects compared to coda temporal variations using microearthquakes doublets in California, *Pure appl. Geophys.,* **134,** 195–228.

Herrmann, R.B., Malagnini, L. & Munafó, I., 2011. Regional moment tensors of the 2009 L'Aquila earthquake sequence, *Bull. seism. Soc. Am.,* **101,** 975–993.

INGV Seismological Data Centre. Rete Sismica Nazionale (RSN). Istituto Nazionale di Geofisica e Vulcanologia (INGV), Italy, 2006. https://doi.org/10.13127/SD/X0FXnH7QfY.

Jin, A. & Aki, K., 1986. Temporal change in coda Q before the Tangshan earthquake of 1976 an the Haicheng earthquake of 1975, *J. geophys. Res.,* **91,** 665–673.

Johnston, D.H., Toksöz, M.N. & Timur, A., 1979. Attenuation of seismic waves in dry and saturated rocks: II. Mechanisms, *Geophysics,* **44**(4), 691–711.

King, T., De Siena, L., Benson, P. & Vinciguerra, S., 2022. Mapping faults in the laboratory with seismic scattering 1: the laboratory perspective, *Geophys. J. Int.,* **232**(3), 1590–1599.

Ktenidou, O.-J., Cotton, F., Abrahamson, N.A. & Anderson, J.G., 2014. Taxonomy of κ: a review of definitions and estimation approaches targeted to applications, *Seismol. Res. Lett.,* **85,** 135–146.

Ktenidou, O.-J., Gelis, C. & Bonilla, L.-F., 2013. A study on the variability of kappa in a borehole: implications of the computation process, *Bull. seism. Soc. Am.,* **103,** 1048–1068.

Lanzano, G., Felicetta, C., Pacor, F., Spallarossa, D. & Traversa, P., 2022. Generic-to-reference rocks scaling factors for the seismic ground motion in Italy, *Bull. seism. Soc. Am.,* **112,** 1583–1606.

Li, G. & Ben-Zion, Y., 2023. Daily and seasonal variations of shallow seismic velocities in southern California from analysis of H/V ratios and autocorrelations of seismic waveforms, *J. geophys. Res.,* **128,** e2022JB025682, doi:10.1029/2022JB025682.

Lolli, B., Gaperini, P. & Boschi, E., 2011. Time variations of aftershock decay parameters of the 2009 April 6 L'Aquila (central Italy) earthquake: evidence of the emergence of a negative exponential regime superimposed to the power law, *Geophys. J. Int.,* **185,** 764–774.

Lu, Y. & Ben-Zion, Y., 2022. Regional seismic velocity changes following the 2019 Mw7.1 Ridgecrest California earthquake from autocorrelations and P/S converted waves, *Geophys. J. Int.,* **228,** 620–630.

Lucente, F.P., De Gori, P., Margheriti, L., Piccinini, D., Di Bona, M., Chiarabba, C. & Piana Agostinetti, N., 2010, Temporal variation of seismic velocity and anisotropy before the 2009 MW 6.3 L'Aquila earthquake, Italy, *Geology,* **38,** 1015–1018.

Malagnini, L., Lucente, F.P., De Gori, P., Akinci, A. & Munafo, I., 2012. Control of pore pressure diffusion on fault failure mode: insights from the 2009 L'Aquila seismic sequence, *J. geophys. Res.,* **117**(B5), doi:10.1029/2011JB008911.

Malagnini, L., Parsons, T., Munafò, I., Mancini, S., Segou, M. & Geist, E.L., 2022. Crustal permeability changes inferred from seismic attenuation: impacts on multi-mainshock sequences, *Front. Earth Sci.,* **10,** doi:10.3389/feart.2022.963689.

Niu, F., Silver, P.G., Daley, T.M., Cheng, X. & Majer, E.L., 2008. Preseismic velocity changes observed from active source monitoring at the Parkfield SAFOD drill site, *Nature,* **454**(7201), 204–208.

Nur, A., 1972. Dilatancy, pore fluids, and premonitory variations of travel times, *Bull. seism. Soc. Am.,* **78,** 1217–1222.

Omori, F., 1894. On the aftershocks of eartquakes, Jour, *J. Coll. Sci.,* **7,** 111–200.

Oth, A., Bindi, D., Parolai, S. & Di Giacomo, D., 2011. Spectral analysis of K-NET and KiK-net data in Japan, part II: on attenuation characteristics, source spectra, and site response of borehole and surface stations, *Bull. seism. Soc. Am.,* **101,** 667–687.

Pacor, F. *et al.* 2016. Spectral models for ground motion prediction in the L'Aquila region (central Italy): evidence for stress-drop dependence on magnitude and depth, *Geophys. J. Int.,* **204,** 697–718.

Parolai, S. & Bindi, D., 2004. Influence of soil-layer properties on *k* evaluation, *Bull. seism. Soc. Am.,* **94,** 349–356.

Peng, Z. & Ben-Zion, Y., 2006. Temporal changes of shallow seismic velocity around the Karadere-Düzce branch of the north Anatolian fault and strong ground motion, *Pure appl. Geophys.,* **163**(2–3), 567–600.

Perron, V., Hollender, F., Bard, P.-Y., Gélis, C., Guyonnet-Benaize, C., Hernandez, B. & Ktenidou, O.-J., 2017. Robustness of kappa (κ) measurement in low-to-moderate seismicity areas: insight from a site-specific study in Provence, France, *Bull. seism. Soc. Am.,* **107,** 2272–2292.

Picozzi, M., Iaccarino, A.G., Spallarossa, D. & Bindi, D., 2023. On catching the preparatory phase of damaging earthquakes: an example from central Italy, *Sci. Rep.,* **13**(14403), doi:10.1038/s41598-023-41625.

Picozzi, M., Spallarossa, D., Bindi, D., Iaccarino, A.G. & Rivalta, E., 2022a. Detection of spatial and temporal stress changes during the 2016 central Italy seismic sequence by monitoring the evolution of the energy index, *J. geophys. Res.,* **127,** e2022JB025100, doi:10.1029/2022JB025100.

Picozzi, M., Spallarossa, D., Iaccarino, A.G. & Bindi, D., 2022b. Temporal evolution of radiated energy to seismic moment scaling during the preparatory phase of the Mw 6.1, 2009 L'Aquila earthquake (Italy), *Geophys. Res. Lett.,* **49,** e2021GL097382, doi:10.1029/2021GL097382.

Poli, P., Marguin, V., Wang, Q., D'Agostino, N. & Johnson, P., 2020. Seasonal and coseismic velocity variation in the region of L'Aquila from single station measurements and implications for crustal rheology, *J. geophys. Res.,* **125,** e2019JB019316, doi:10.1029/2019JB019316.

Poupinet, G., Ellsworth, W.L. & Frechet, J., 1984. Monitoring velocity variations in the crust using earthquake doublets: an application to the Calaveras Fault, California, *J. geophys. Res.,* **89**(B7), 5719–5731.

Savage, M.K., 2010. The role of fluids in earthquake generation in the 2009 Mw 6.3 L'Aquila, Italy, earthquake and its foreshocks, *Geology,* **38,** 1055–1056.

Scherbaum, F., 1990. Combined inversion for the three-dimensional Q structure and source parameters using microearthquake spectra, *J. geophys. Res.,* **95,** 12 423–12 438.

Scholz, C.H., Sykes, L.R. & Aggarwal, Y.P., 1973. Earthquake prediction: a physical basis, *Science,* **181,** 803–809.

Scognamiglio, L., Tinti, E., Michelini, A., Dreger, D.S., Cirella, A., Cocco, M., Mazza, S. & Piatanesi, A., 2010. Fast determination of moment tensors and rupture history: what has been learned from the 6 April 2009 L'Aquila earthquake sequence, *Seismol. Res. Lett.,* **81,** 892–906.

Sibson, R.H., 1992. Implications of fault-valve behaviour for rupture nucleation and recurrence, *Tectonophysics,* **211,** 283–293.

Sibson, R.H., 2009. Rupturing in overpressured crust during compressional inversion—the case from NE Honshu, Japan, *Tectonophysics,* **473,** 404–416.

Singh, S.K., Apsel, R.D., Fried, J. & Brune, J.N., 1982. Spectral attenuation of SH waves along the imperial fault, *Bull. seism. Soc. Am.,* **72,** 2003–2016.

Soldati, G., Zaccarelli, L., Faenza, L. & Michelini, A., 2015. Monitoring of crustal seismic velocity variations in the L'Aquila fault zone inferred from noise cross-correlation, *Geophys. J. Int.,* **202,** 604–611.

Terakawa, T., Zoporowski, A., Galvan, B. & Miller, S.A., 2010. High-pressure fluid at hypocentral depths in the L'Aquila region inferred from earthquake focal mechanisms, *Geology,* **38,** 995–998.

Tinti, E., Scognamiglio, L., Cirella, A. & Cocco, M., 2014. Up-dip directivity in near-source during the 2009 L'Aquila mainshock, *Geophys. J. Int.,* **198,** 1618–1631.

Tisato, N. & Quintal, B., 2014. Laboratory measurements of seismic attenuation in sandstone: strain versus fluid saturation effects strain and saturation effects, *Geophysics,* **79**(5), WB9–WB14.

Toksoz, M.N., Johnston, D.H. & Timur, A., 1979. Attenuation of seismic waves in dry and saturated rocks: I. Laboratory measurements, *Geophysics,* **44**(4), 681–690.

Townend, J., 2006. What do faults feel? Observational constraints on the stresses acting on seismogenic faults, in *Earthquakes: Radiated Energy and the Physics of Faulting,* Vol. **170,** pp. 313–327, eds Abercrombie, R.E. *et al.*, Geophysical Monograph Series, American Geophysical Union.

Valoroso, L., Chiaraluce, L., Piccinini, D., Di Stefano, R., Schaff, D. & Waldhauser, F., 2013. Radiography of a normal fault system by 64 000 high-precision earthquake locations: the 2009L'Aquila (central Italy) case study, *J. geophys. Res.,* **118,** doi:10.1002/jgrb.50130.

Van Houtte, C., Drouet, S. & Cotton, F., 2011. Analysis of the origins of K (Kappa) to compute hard rock to rock adjustment factors for GMPEs, *Bull. seism. Soc. Am.,* **101,** 2926–2941.

Walters, R.J. *et al.* 2009. The 2009 L'Aquila earthquake (central Italy): a source mechanism and implications for seismic hazard, *Geophys. Res. Lett.,* **36**(L17), doi:10.1029/2009GL039337.

Wessel, P. & Smith, W.H., 1998. New, improved version of Generic Mapping Tools released. *Eos,* **79**(47), 579.

Winkler, K.W. & Nur, A., 1982. Seismic attenuation: effects of pore fluids and frictional-sliding, *Geophysics,* **47**(1), 1–15.

Zhao, D. & Negishi, H., 1998. The 1995 Kobe earthquake: seismic image of the source zone and its implications for the rupture nucleation, *J. geophys. Res.,* **103,** 9967–9986.